JOURNAL OF GEOPHYSICAL RESEARCH, VOL. 101, NO. B11, PAGES 25,139–25,147, NOVEMBER 10, 1996

Evaluating hysteresis in earth materials under dynamic resonance

Abraham Kadish and Paul A. Johnson[1]
Earth and Environmental Sciences Division, Los Alamos National Laboratory, Los Alamos, New Mexico

Bernard Zinszner
Institut Français du Pétrole, Rueil Malmaison, France

Abstract. A lumped parameter model is derived for studying hysteretic effects in resonant bar experiments on rock. The model uses equations of state obtained by approximating closed hysteresis loops in the stress-strain plane by parallelograms. The associated approximate nonlinear state relations have a sound speed (modulus) that takes two values. Assuming hysteresis and discrete memory to be the primary nonlinear mechanisms, periodic solutions corresponding to these equations of state are obtained analytically for single-frequency continuous wave drivers, and their frequency spectral densities are analyzed. In this simple approximation, if hysteretic contributions to the signal speed are a correction to the linear elastic signal speed (i.e., the parallelogram is narrow), the model predicts that the spectral density at even multiples of the source frequency is zero, and an approximate "pairing" of amplitudes is predicted for odd harmonic multiples. Comparison of the model spectrum with experimental data shows the model to be qualitatively correct. We conclude that hysteresis is an important mechanism in rocks. We consider the model to be a prototype.

Introduction

Nonlinear elastic wave propagation experiments have been conducted at Los Alamos National Laboratory and the Institut Français du Pétrole as part of an effort to determine the nonlinear state parameters in earth materials [e.g., *Meegan et al.*, 1993; *Johnson et al.*, 1996; B. Zinszner et al., Influence of change in physical state on elastic nonlinear response in rock: Effects of effective pressure and water saturation, submitted to *Journal of Geophysical Research*, 1996]. Three types of experiments are being conducted with this goal in mind: static stress-strain, dynamic pulse propagation, and dynamic resonance experiments [see, e.g., *Johnson and Rasolofosaon*, 1996]. The dynamic experimental evidence suggests that more familiar approaches to modeling a nonlinear resonant system, such as the Duffing equation [see *Stoker*, 1950], do not predict the empirical behavior of the harmonic spectrum and resonant frequency alteration for earth materials [*Guyer et al.*, 1995a, b; *Johnson et al.*, 1996]. That is, classical predictions of harmonic distribution and resonant frequency shift as a function of drive amplitude in resonance experiments on earth materials do not match observation. This same conclusion has also been obtained from pulse mode wave experiments [*Ten Cate et al.*, 1996; *Van Den Abeele and Johnson*, 1996; *Kadish*, 1995; *Kadish et al.*, 1996].

It is clear from static tests on earth materials that hysteresis and discrete memory are characteristic [*Boitnott*, 1993; *Holcomb*, 1978, 1981; *Gardner et al.*, 1965; *Birch*, 1966]. These two characteristics, together with the poor predictions obtained from classical nonlinear wave theory [*Guyer et al.*, 1995a, b] suggest that hysteresis and discrete memory may play an important role in propagating and standing waves. There is considerable experimental evidence suggesting that hysteresis and discrete memory and/or other nonlinear phenomena strongly effect propagating and standing waves at strain levels as low as 10^{-7} under ambient conditions [*Ostrovsky*, 1991; *Guyer et al.*, 1995a; *Johnson et al.*, 1996].

We introduce a simple lumped parameter model to evaluate the effects of hysteresis in resonant bar experiments. It will be demonstrated that the lumped parameter model (also "zero dimensional") predicts resonant periodic motions whose spectral amplitudes exhibit qualitative properties similar to those observed in experiments. The term hysteresis is usually employed in two contexts: history-dependent multivalued state relations in nonlinear materials (e.g., between stress and strain in rocks and between the magnetic field and magnetic induction in magnetic materials) and the discontinuous relations observed between input and output experimental parameters (e.g., frequency versus amplitude) in driven nonlinear systems. Both of these hysteretic phenomena are observed in rocks. Because the latter form is common to almost all nonlinear systems (e.g., Duffing's equation), its presence cannot be used to deduce the existence of a multivalued state relation. The lumped parameter model described in this paper uses a multivalued stress-strain relation that is amenable to mathematical analysis of oscillations driven in resonant bar experiments. Although the modeling procedure accommodates other nonlinearities, the multivalued nature of the state relation is the only nonlinearity considered here in order to facilitate analysis. (It is also the only source of dissipation considered.) Consequently, one does not expect complete quantitative agreement with data from nonlinear resonant bar experiments. However,

[1]Also at Department d'Acoustique Physique, Université Pierre et Marie Curie (Paris 6), Paris.

Paper number 96JB02480.
0148-0227/96/96JB-02480$09.00

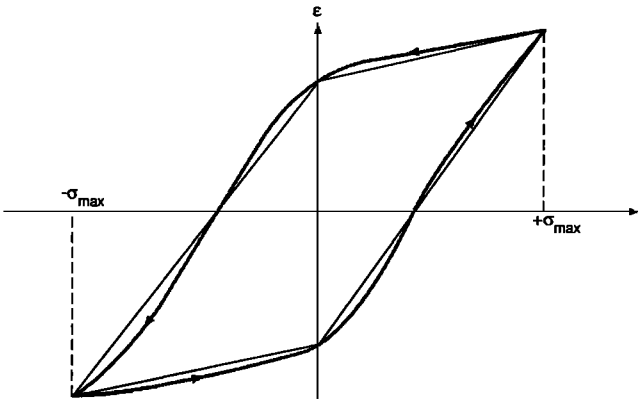

Figure 1. The model hysteresis loop used in this paper, for the special case where $\sigma_0 = 0$ (parallelogram), and a more physically realistic version (bold line) in stress-strain (σ-ε) space. For the approximating parallelogram, there are precisely two signal speeds (equivalently elastic moduli). The arrowheads indicate direction of increasing time.

the model does allow a qualitative determination of the relative strengths of hysteresis vis-à-vis other nonlinear effects. In particular, the hysteretic spectral signature exhibits unique and easily identified properties for weak nonlinearity.

In the following section an overview of the theory is provided, but the details have been placed in the appendices. Spectral data from recent resonant bar experiments are presented in the subsequent section. A discussion of the lumped parameter model and the pertinent spectral properties it predicts for resonant bar experiments follows the data section.

Wave Equations With Hysteresis

One-dimensional nonlinear pulse propagation in ideal and nonideal elasticity is governed by coupled wave equations for the stress σ and particle velocity v. The local signal speeds, c_{signal}, are given by

$$c_{\text{signal}} \equiv \sqrt{\frac{d\sigma/d\varepsilon}{\rho^*}} \tag{1}$$

where ε is the local strain and ρ^* is the mass density of the unstressed sample. In nonideal materials the stress-strain relation is not one-to-one. Hysteresis and other plasticity phenomena result in multivalued state relations (in the remainder of this paper, use of the term hysteresis will be restricted to mean phenomena associated with multivalued state relations as opposed to hysteresis of the resonance frequency-amplitude response). An example of such a relation is illustrated in Figure 1. The curvilinear loop in the figure represents an empirical path. Arrows along the path indicate direction with increasing time. The counterclockwise direction corresponds to hysteresis being dissipative. The parallelogram in the figure is a convenient approximation, which is discussed in detail below. Sufficiently simple periodic evolution of stress and strain results in repetition of closed loops of the type shown in Figure 1. As illustrated by the curvilinear loop, hysteretic state relations usually exhibit discontinuous variations in local signal speed (or modulus) when the time derivative of stress changes sign. The material responds differently to increases in stress than it does to decreases. The hysteretic response is generally attributed to the compliant features in the material such as cracks, grain-to-grain contacts, etc. The discontinuities in signal speed produce shocks not seen in the limit of ideal elasticity. The shocks are space-time paths across which derivatives of stress and particle velocity are not continuous. Evidently, it is necessary to account for local histories of stress for accurate numerical simulations of pulse propagation in hysteretic materials.

The simplest mathematical models of signal speed in a hysteretic material are obtained by approximating curvilinear hysteresis loops by parallelograms, an example of which is illustrated in Figure 1. In this paper approximations of the form

$$\frac{1}{\rho^*}\frac{d\sigma}{d\varepsilon} = c_0^2\left(1 + \left[\operatorname{sgn}\left\{\frac{\partial(\sigma - \sigma_0)^2}{\partial t}\right\}\right]h_{\pm}\right) \tag{2}$$

are used. Here, c_0^2 is the square of the constant "elastic" signal speed of the medium, and the h are hysteresis constants (subscripts refer to the sign of the sgn function).

Effectively, the medium behaves like two different elastic materials. The sgn function and the $h_{\pm}$ provide a mathematical prescription for switching between one material and the other. The signs of the hysteresis constants determine dissipative properties of hysteresis. If they are negative, as will be assumed in this paper, hysteresis is a dissipative mechanism. It is the only dissipative mechanism and nonlinear effect included in this treatment. The sgn function of the time derivative of $(\sigma - \sigma_0)^2$ determines the times at which the change in elastic behavior occurs. The values of the hysteresis constants $h_{\pm}$ together with the elastic signal speed determine the slopes (i.e., moduli) of the stress strain relation on the parallelogram approximation to the hysteresis loop as shown in Figure 1 for the special case $\sigma_0 = 0$. During propagation, the speeds are piecewise constant in time, greatly simplifying analysis.

Following the arrowheads on the curvilinear loop indicating the direction of time in Figure 1, abrupt changes in slope occur when $(\sigma - \sigma_0)^2$ is maximum, $\sigma^2_{\max}$. These abrupt changes are physical. (When the maximum is achieved, the time derivative of $(\sigma - \sigma_0)^2$ changes sign and the material switches elastic states.) Figure 1 also shows that the slopes at common values of σ depend on whether $(\sigma - \sigma_0)^2$ is increasing or decreasing with time.

With the parallelogram approximation to the closed loop, discontinuities in signal speed also occur when $\sigma - \sigma_0$ changes sign and require special treatment. These discontinuities are not physical. Their presence is a price one pays for the mathematical simplification gained by introducing the parallelogram approximation to the true hysteresis loop. Equation (2) could be made more physically realistic by smoothing to provide continuous signal speeds at $\sigma = \sigma_0$, as illustrated by the curvilinear path in Figure 1; however, the analysis is much more difficult and, we believe, would not add significantly to the physics contained in the model. Equation (2) may be regarded as a limiting case of expressions not having this discontinuity. In order to avoid nonphysical shocks when using (2), continuity of first derivatives of stress and particle velocity will be imposed when $\sigma - \sigma_0$ changes sign.

In Appendix A, a lumped parameter model for temporal oscillations driven in resonant bar experiments is derived from propagation equations with signal speeds modeled using (2). The nonlinear oscillator equations for the evolution of the dimensionless scaled lumped stress $s(t)$ and particle velocity $w(t)$ are (see Appendix A)

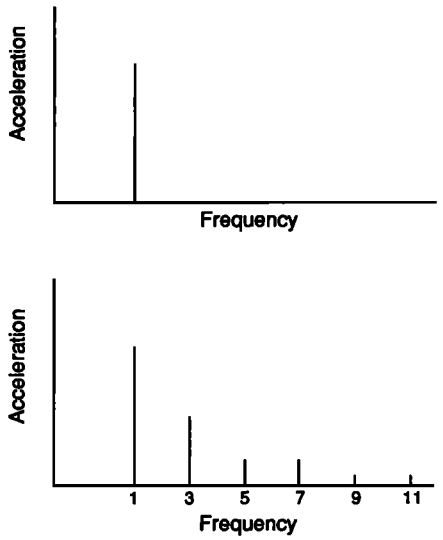

Figure 2. (top) Single-frequency source spectrum, and (bottom) detected spectrum of the type predicted.

$$\frac{d^2}{dt^2}\begin{pmatrix} s^{\pm}(t) \\ w^{\pm}(t) \end{pmatrix} + (1 \pm \delta)^2\Omega^2\begin{pmatrix} s^{\pm}(t) \\ w^{\pm}(t) \end{pmatrix} = -\begin{pmatrix} \dfrac{dv(0,t)}{dt} \\ \dfrac{d^2v(0,t)}{dt^2} \end{pmatrix} \qquad (3)$$

where $v(0, t)$ is the particle velocity applied at the end of the bar at $z = 0$. Here we note that both δ and Ω are positive constants that are properties of the material. Ω is an angular frequency, and δ is a hysteretic strength parameter. The plus and minus signs appearing in front of δ and as superscripts of $s(t)$ and $w(t)$ are those of the sgn function in (2).

In the absence of hysteresis, $\delta = 0$, and application of a source function $v(0, t)$ having angular frequency Ω produces unbounded stresses and particle velocities. For $0 < \delta < 1$ the model of the hysteresis effect is dissipative, and solutions to (3) are bounded. In Appendix B, (3) is solved for $\delta \ll 1$ (weak hysteresis) when $v(0, t)$ is periodic with angular frequency Ω. In Appendix C the acceleration frequency spectrum of those solutions is analyzed. Characteristic properties of solutions in resonance with the driver are that to order 1 in the asymptotic expansion in small δ, (1) terms corresponding to even multitudes of Ω are absent, i.e., have zero amplitude (see equation (C3)), and (2) there is an approximate pairing of the acceleration amplitudes of terms corresponding to higher odd multiples of Ω (i.e., ratios of the amplitudes of the 5Ω and 7Ω terms are equal to 1 within 2%, while those of the 9Ω and 11Ω terms, etc., are equal to 1 within <1% (see equations (C5) and (C6)).

These results are illustrated qualitatively in Figure 2. The top portion of the figure shows a the spectrum of the driver. The bottom portion of the figure shows a detected spectrum of the type predicted by the model.

Comparison With Experimental Data

A schematic of a resonant bar experiment is shown in Figure 3a along with the typical character of nonlinear response in resonance in rock (Figure 3b). The bar, occupying $0 < z < L$, is driven at $z = 0$ with a periodic velocity $v(0, t)$ while the end at $z = L$ is stress free, $\sigma(L, t) = 0$. The resonance peak shifts downward with increasing drive level as a result of the nonlinear response of the material. The plot also illustrates the hysteretic nature of the frequency-amplitude response of a resonant bar driven at nonlinear levels; the upgoing and downgoing frequency curves are very different from each other when the bar is driven at nonlinear levels.

Figure 4 illustrates experimental harmonic measurements from three rock types: Fontainebleau sandstone, Lavoux limestone, and Meule sandstone [see, e.g., *Lucet and Zinszner*, 1992]. The detected acceleration is plotted on the horizontal

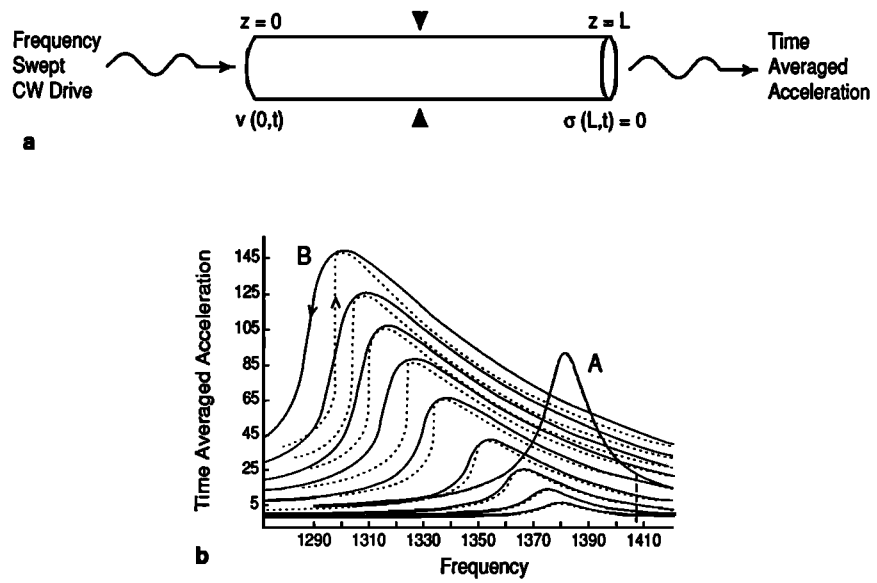

Figure 3. Illustrations of (a) resonant bar experimental configuration and (b) typical resonant frequency response. In the bottom plot, dotted (solid) curves show the response as the source frequency is increased (decreased) while the amplitude is held constant. The curve labeled "A" is an amplification of the response of a very low amplitude source in order to illustrate its behavior. The peak at B illustrates the response to the largest drive level.

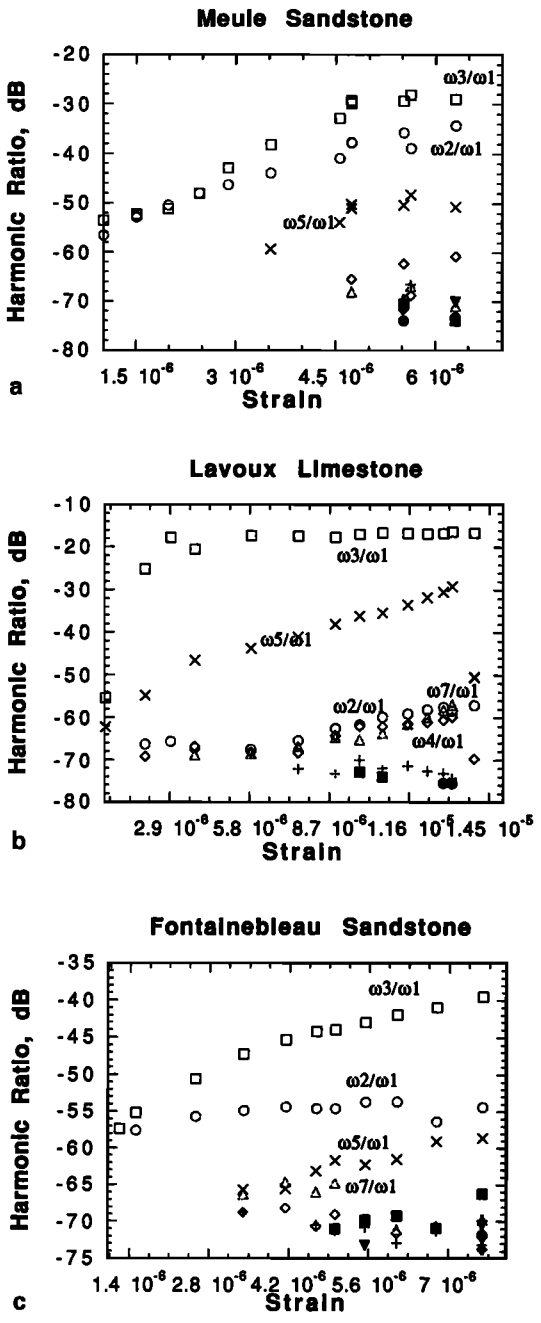

Figure 4. Illustration of Young's mode resonant bar experimental spectral ratios for three different rock samples: (a) Meule sandstone, (b) Lavoux limestone, and (c) Fontainebleau sandstone. Note the dominance in amplitude of the third harmonic over the second in each case. In the limestone, both the third and fifth harmonics are larger than the second harmonic. The other symbols represent higher harmonics.

axis, and the harmonic ratios, $\omega i/\omega 1$, of the ith frequency multiple of the source frequency are plotted on the vertical axis. The harmonic amplitudes were obtained from a Fourier transform of the time signal measured at peak resonance for each successive resonance peak with increasing drive level. The data are reliable to −72.25 dB. The rocks were under ambient conditions for the measurements.

The three rock types have very different mineralogy, crack, and grain contact structure; however, they all illustrate typical characteristics of rock. As shown in Figure 4, for instance, the third harmonic amplitude is generally the largest. This is a very common observation in rocks in general. In all of the rock samples shown in Figure 4 there is a dominance in amplitude of the odd harmonics over the neighboring even harmonics; i.e., $\omega 3$ is almost always larger than $\omega 2$ and $\omega 4$, $\omega 5$ is always larger than $\omega 4$ and $\omega 6$, etc.

If hysteresis is important, the theory of the preceding section should be most accurate at low amplitude where other sources of nonlinearity are less important. There were no data available at very low amplitude. Consequently, linear fits of the available data were extrapolated to low amplitude. Figure 5 illustrates ratios of $\omega 7/\omega 5$ for the three rock types obtained from the data illustrated in Figure 4, together with a least squares linear fit. Extrapolation of the linear fits to zero acceleration yields ratios of about 1.77 for Fontainebleau, 0.082 for Lavoux, and 0.27 for Meule. Note that as the amplitude of the drive decreases, the ratios increase in all cases. While these extrapolations do not exhibit the predicted pairing of harmonics (ratio = 1), the data and slope of the fit are compatible with hysteresis dominating other nonlinear effects at low amplitude. If only classical nonlinearities were present, these ratios would decrease to zero with decreasing amplitude.

Although the theory presented here does predict general characteristics such as the dominance in amplitude of neighboring odd harmonics, modeling of the state relation must be extended to include other nonlinear phenomena as well.

Discussion and Conclusions

Lumped parameter models of resonant bar experiments (equations (A1)–(A4)) were obtained from one-dimensional equations of conservation of mass and momentum for nonideal elastic materials whose state relation is hysteretic. Periodic solutions were obtained analytically, and their spectra were compared with the experimental data.

The lumped parameter models were applied to materials driven in resonance from one boundary and free at the other. This configuration is the one used in nonlinear resonant bar experiments. Periodic solutions driven by a single-frequency source were obtained for approximating stress-strain loops. For analytical purposes, the simplest closed hysteresis loop in stress-strain coordinates is a parallelogram because it corresponds to a stress-strain relation with only two signal speeds. For weak hysteresis, the theory predicts the amplitude of resonant motions to scale inversely with the strength of the hysteresis. (This is because hysteresis was the only damping mechanism included in this treatment; see equation (C3)). In addition, at odd multiples of the source frequency, the spectra of these solutions exhibit pairing: the ratios of the amplitudes of the seventh to fifth, eleventh to ninth, etc., are very close to unity. Because the only nonlinearity present is hysteresis, even harmonics have zero amplitude in this approximation. If other nonlinearities were included in the model, e.g., nonconstant elastic signal speed, even harmonics would be present and the pairing of odd harmonic amplitudes would be weakened.

The pairing of odd harmonic amplitudes predicted by the theory was qualitatively confirmed by experiment; i.e., linear extrapolation of the $\omega 7$ to $\omega 5$ ratio to low-amplitude drive was consistent with theory. (Note that higher frequencies could not be used because these data were beneath the noise floor.) The linear extrapolation to low amplitude is not conclusive; however, as is shown in Figure 5, the extrapolations indicate an

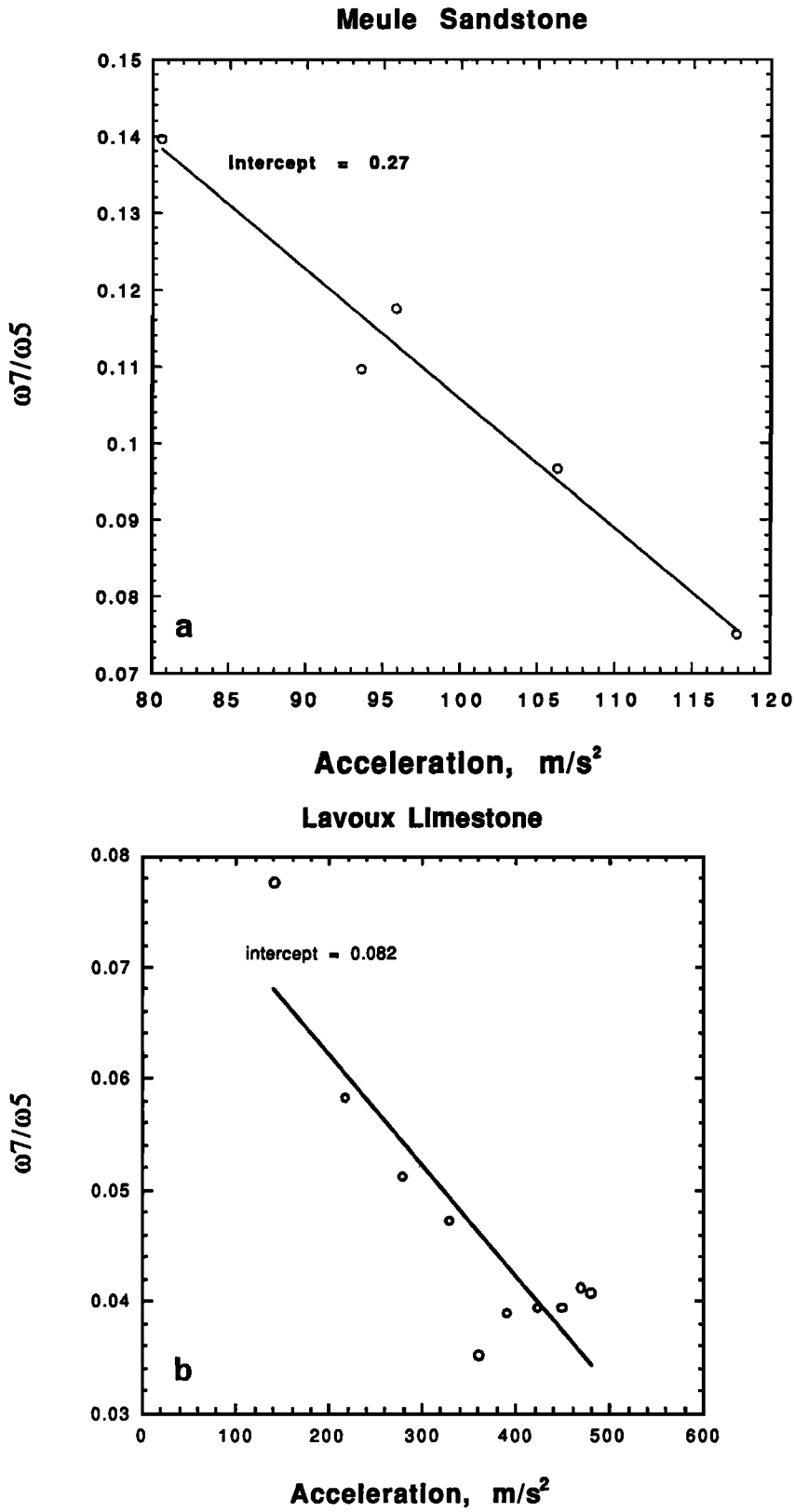

Figure 5. Ratio of measured harmonic amplitudes $\omega 7/\omega 5$ versus detected acceleration for (a) Meule sandstone, (b) Lavoux limestone, and (c) Fontainebleau sandstone. Linear fit shown and intercept of fit noted on plots.

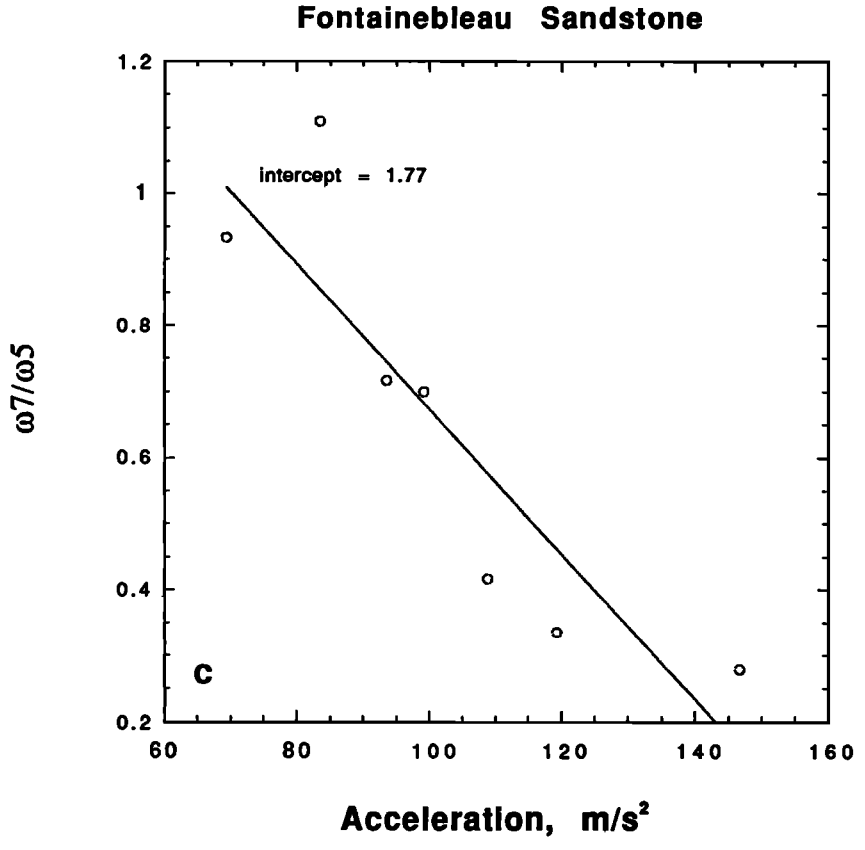

Figure 5. (continued)

increasing ratio as amplitude decreases. In the absence of hysteresis, ratios of spectral amplitudes would be expected to approach zero with decreasing amplitude on the basis of classical perturbation analysis [*Stoker*, 1950]. Even with hysteresis, at low drive levels the absolute harmonic amplitudes approach zero, but their ratio, according to this model, does not. Consequently, the extrapolations of the observations are consistent with hysteresis being a dominant mechanism and suggest that care should be taken when applying classical perturbation methods to hysteretic materials.

The lumped parameter model derived here can be used with more complete state relations. The only dissipative and nonlinear mechanism considered was that due to hysteresis. The model can accommodate other damping mechanisms and nonlinearities. Further development of the model will seek a more complete account of observed spectral properties by expanding the prototype to include additional phenomena.

Appendix A: Lumped Parameter Model

The simplest one-dimensional model for studying compressional wave propagation in elastic and elastic-plastic media is the first-order 2 × 2 system consisting of the equations of continuity and force balance for the stress, $\sigma(x, t)$, and particle velocity, $v(x, t)$ (the laboratory position coordinate is x, and time is t). In Lagrangian coordinates (i.e., coordinates fixed in the material),

$$\frac{1}{d\sigma/d\varepsilon}\frac{\partial \sigma}{\partial t} - \frac{\partial v}{\partial z} = 0 \qquad \rho^* \frac{\partial v}{\partial t} - \frac{\partial \sigma}{\partial z} = 0 \qquad \text{(A1)}$$

where $\varepsilon(z, t)$ is the strain; a state, or stress-strain, relation between σ and ε has been assumed; and ρ^* is the mass density in the absence of stress, where the laboratory coordinate x of an element is a function of its initial position, or Lagrangian coordinate z, so that $x = x(z, t)$ (see Figure 3). The particle velocity is the partial derivative of x with respect to t.

In this appendix and the ones that follow, the expression for $d\sigma/d\varepsilon$ given by equation (2) of the main text is used. In this appendix a lumped parameter model for resonant bar experiments is derived using (A1). The method, described below, is equivalent to a spatial averaging of (A1).

The lumped parameters for the particle velocity and stress for a bar as illustrated in Figure 3a will be denoted by $v(t)$ and $\sigma(t)$, respectively. It will be assumed that a driving particle velocity, $v(0, t)$ is applied at one end of the bar, $z = 0$, and that the other end of the bar, $z = L > 0$, is stress-free. We reduce the dimensionality of the system given in (A1) by replacing spatial derivatives by difference quotients using the gradient scale lengths Z_v and Z_σ defined by

$$\frac{\partial}{\partial z} v(z, t) \approx \frac{v^{\pm}(t) - v(0, t)}{Z_v^{\pm}}$$

$$\frac{\partial}{\partial z} \sigma(z, t) \approx \frac{\sigma^{\pm}(L, t) - \sigma(t)}{Z_\sigma^{\pm}} = -\frac{\sigma^{\pm}(t)}{Z_\sigma^{\pm}}, \qquad \text{(A2)}$$

respectively. The superscripts refer to the sign of the sgn function in (2). The time derivatives of (A1) are replaced by time derivatives at values of stress and particle velocity at values between the lumped parameter and known boundary values

$$\frac{\partial}{\partial t} v(z, t) \approx \frac{d}{dt}\left[\vartheta_v^{\pm} v(0, t) + (1 - \vartheta_v^{\pm}) v^{\pm}(t)\right]$$

$$\frac{\partial}{\partial t}\sigma(z, t) \approx \frac{d}{dt}\left[\vartheta_\sigma^{\pm}\sigma(t) + (1 - \vartheta_\sigma^{\pm})\sigma^{\pm}(L, t)\right] = \frac{d}{dt}\left[\vartheta_\sigma^{\pm}\sigma(t)\right]. \tag{A3}$$

The ϑ are intermediate value parameters (i.e., if the ϑ are assigned different values between zero and one, the quantities being differentiated take values between the boundary data and the lumped parameters). Substituting (A2) and (A3) in (A1) yields a coupled system of first-order ordinary differential equations for the lumped particle velocity parameter $v(t)$ and stress parameter $\sigma(t)$.

$$\frac{d}{dt}\left[\frac{\vartheta_\sigma^{\pm}\sigma(t)}{\rho^*}\right] - \frac{1}{\rho^*}\left(\frac{d\sigma}{d\varepsilon}\right)^{\pm}\left[\frac{v^{\pm}(t) - v(0, t)}{Z_v^{\pm}}\right] = 0$$

$$\frac{d}{dt}\left[\vartheta_v^{\pm} v(0, t) + (1 - \vartheta_v^{\pm}) v^{\pm}(t)\right] + \frac{\sigma^{\pm}(t)}{\rho^* Z_\sigma^{\pm}} = 0 \tag{A4}$$

Constraints exist that limit the number of independent gradient scale lengths and intermediate value parameters in the system. Because the terms that are not time derivatives are integrable when the derivative of the stress changes sign, the terms being differentiated are continuous. This implies that there are only two independent intermediate value parameters

$$\vartheta_v^{+} = \vartheta_v^{-} \equiv \vartheta_v \qquad \vartheta_\sigma^{+} = \vartheta_\sigma^{-} \equiv \vartheta_\sigma \tag{A5}$$

Moreover, because the time derivative of $\sigma(t)$ is continuous when $\sigma(t)$ changes sign, the first relation in (A4) yields the constraint

$$\left(\frac{1}{\rho^* Z_v}\frac{d\sigma}{d\varepsilon}\right)^{+} = \left(\frac{1}{\rho^* Z_v}\frac{d\sigma}{d\varepsilon}\right)^{-} = \frac{C^2}{Z_v} \tag{A6}$$

Equation (A6), together with the second relation in (A5) and continuity of $v(t)$, implies that the first derivative of the $\sigma(t)$ is a continuous function of time. It must therefore vanish at maxima and minima of $\sigma(t)$. At stationary values of $\sigma(t)$, the $v(t) - v(0, t) = 0$.

Differentiation of (A4) using (A5) and (A6) yields oscillator equations for the stress and particle velocity parameters:

$$\frac{d^2}{dt^2}\left(\frac{\sigma^{\pm}(t)}{\rho^*}\right) + \Omega_{\pm}^2\left(\frac{\sigma^{\pm}(t)}{\rho^*}\right) = -\frac{1}{\vartheta_\sigma(1 - \vartheta_v)}\frac{C^2}{Z_v}\frac{d}{dt} v(0, t)$$

$$\frac{d^2}{dt^2}(v^{\pm}(t) - v(0, t)) + \Omega_{\pm}^2(v^{\pm}(t) - v(0, t)) \tag{A7}$$

$$= -\frac{1}{(1 - \vartheta_v)}\frac{d^2}{dt^2} v(0, t)$$

where

$$\Omega_{\pm}^2 \equiv \frac{1}{\vartheta_\sigma(1 - \vartheta_v)}\frac{C^2}{Z_v}\left(\frac{1}{Z_\sigma^{\pm}}\right)$$

$$\equiv \frac{1}{\vartheta_\sigma(1 - \vartheta_v)}\frac{C^2}{Z_v}\frac{(1 \pm \delta)^2}{Z_\sigma} \equiv \Omega^2(1 \pm \delta)^2 \tag{A8}$$

defines the frequency parameters appearing in (A7) and in equation (3) of the main text. The scaled lumped parameters appearing in (3) are obtained from the definitions

$$\left(\frac{\sigma^{\pm}(t)}{\rho^*}\right) \equiv \frac{1}{\vartheta_\sigma(1 - \vartheta_v)}\frac{C^2}{Z_v} s^{\pm}(t)$$

$$(v^{\pm}(t) - v(0, t)) \equiv \frac{1}{(1 - \vartheta_v)} w^{\pm}(t) \tag{A9}$$

Assuming Ω^2 is positive, we must have $0 < \delta$ for hysteresis to be dissipative. Therefore the gradient scale length associated with an increasing magnitude of stress is less than that associated with a decreasing magnitude of stress, and the principle dynamic effect of hysteresis in the model is seen to be associated with an abrupt change in effective gradient scale lengths for stress. Hysteresis will be said to be weak if the difference in these gradient scale lengths is small (i.e., if δ is small).

Appendix B: Determination of the Stress

In this appendix we obtain an asymptotic expansion for the stress when δ is small and the displacement source term for the resonant bar is $v(0, t) = -V \sin \Omega t$. The periodic stress generates a simple closed parallelogram in the stress-strain plane (see Figure 1). To simplify the presentation, we introduce dimensionless parameters τ, $S(\tau)$, and $W(\tau)$ in place of time, stress, and particle velocity, given by

$$\tau \equiv \Omega t$$

$$S^{\pm}(\tau) \equiv \vartheta_\sigma(1 - \vartheta_v)\frac{Z_v \Omega \sigma^{\pm}(\tau)}{V\rho^* C^2} \tag{B1}$$

$$W^{\pm}(\tau) \equiv (1 - \vartheta_v)\frac{[v^{\pm}(\tau) - v(0, \tau)]}{V}$$

For clarity, the same physical lumped parameter symbols have been used even though the independent variable t has been replaced by τ. With these variables, the equation for the dimensionless stress (see (A7)) is

$$\frac{d^2}{d\tau^2} S^{\pm}(\tau) + (1 \pm \delta)^2 S^{\pm}(\tau) = \cos \tau \tag{B2}$$

$W(\tau)$ may be found from $S(\tau)$ using (A4).

Our procedure for determining $S(\tau)$ with period 2π is as follows: We use a clock for times T given by

$$\tau = T + \Phi - \pi/2 \tag{B3}$$

which is set so that $dS(T)/dT = 0$ at $T = \pm\pi/2$ with $dS(T)/dT > 0$ on the half-period interval $-\pi/2 < T < +\pi/2$, and we require $S(-\pi/2) = -S(+\pi/2)$. The phase Φ depends upon δ. Let T_0 be the time (to be determined) in the interval $-\pi/2 < T < +\pi/2$ at which $S(T_0) = 0$. Requiring periodicity, the stress on $-\pi/2 < T < +\pi/2$ and (B2) implies that the continuation onto $+\pi/2 < T < +3\pi/2$ is given by $S(T) = -S(T - \pi)$ (see Figure B1), with obvious periodic continuation of the solution for all times. Again using the same symbol for the stress parameter,

$$\frac{d^2}{dT^2} S^{\pm}(T) + (1 \pm \delta)^2 S^{\pm}(T) = -\sin(T + \Phi) \tag{B4}$$

The solutions to (B4) for $-\pi/2 < T < +\pi/2$ are given by

$$[(1 \pm \delta)^2 - 1]S^{\pm}(T) = A^{\pm} \cos[(1 \pm \delta)(T - T_0)]$$

$$+ B^{\pm} \sin[(1 \pm \delta)(T - T_0)] + \sin(T + \Phi) \tag{B5}$$

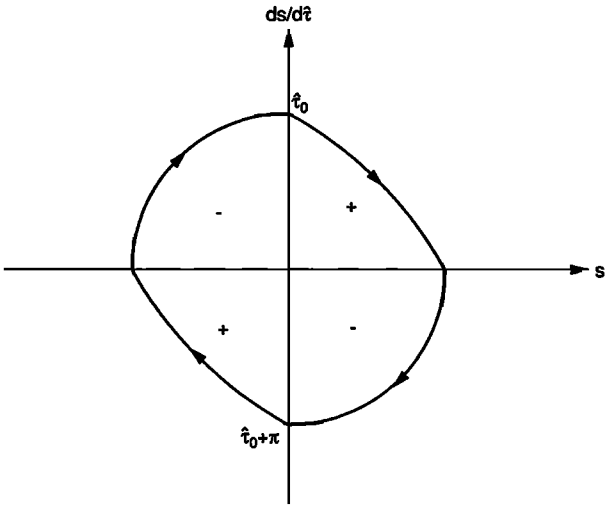

Figure B1. Phase space representation of the closed hysteresis loop from Figure 1 for the evolution of the dimensionless stress. Arrowheads on the curve indicate the direction of variation. The plus and minus signs in quadrants correspond to the sign of the product of stress and its derivative in the quadrant. The period is 2π. Two points on the solution path lying on the same straight line though the origin are equally distant from the origin and separated in time by π.

Equation (B5) contains six δ-dependent constants, $A^{\pm}$, $B^{\pm}$, T_0 and Φ, that must satisfy the six symmetry and continuity constraints on the interval:

$$S^{-}(-\pi/2) = -S^{+}(+\pi/2), \qquad \frac{d}{dT}S^{+}(T_0) = \frac{d}{dT}S^{-}(T_0),$$

$$S^{\pm}(T_0) = 0, \qquad \frac{d}{dT}S^{+}(+\pi/2) = \frac{d}{dT}S^{-}(-\pi/2) = 0 \tag{B6}$$

For $\delta \ll 1$, (B6) yields

$$T_0 = \left(\frac{\pi}{2} - \frac{2}{\pi}\right)\delta + O(\delta^2) \qquad \Phi = \tfrac{3}{2}T_0 + O(\delta^2)$$

$$S^{+}(T) = \frac{\pi/4}{\delta}\sin T + \frac{1}{2}\left\{\left(T - \frac{\pi}{2}\right)\sin T + \left[1 - \frac{\pi}{2}\left(\frac{\pi}{2} - T\right)\right]\cos T\right\} + O(\delta) \tag{B7}$$

$$S^{-}(T) = \frac{\pi/4}{\delta}\sin T + \frac{1}{2}\left\{\left(T + \frac{\pi}{2}\right)\sin T + \left[1 - \frac{\pi}{2}\left(\frac{\pi}{2} + T\right)\right]\cos T\right\} + O(\delta)$$

The linear time dependence in the asymptotic expansions for $s(T)$ in δ is due to expansions of trigonometric functions having δ-dependent arguments.

Appendix C: Acceleration Frequency Spectrum

The time series and spectra from resonant bar experiments are usually obtained from accelerometer measurements. In this appendix we use (A4) and the stress given by (B7) to obtain the lead terms up to order 1 in the expansion of the acceleration spectrum for weak hysteresis.

In terms of the dimensionless parameters of Appendix B, (A4) becomes

$$W^{\pm}(T) = \frac{d}{dT}S^{\pm}(T) \qquad (1 \pm \delta)^2 S^{\pm}(T) = \frac{d}{dT}W^{\pm}(T) \tag{C1}$$

Since the dimensionless stress and strain have period 2π in T, it is natural to represent them as a Fourier series in sine and cosine functions periodic in T on $-\pi < T < +\pi$. Odd-numbered harmonics will not appear in the series because $S(T + \pi) = -S(T)$.

Up to and including terms of order one, the first equation of (C1) is

$$\frac{d}{dT}\left[\frac{(1 - \vartheta_v)v^{\pm}(T)}{V}\right] = (1 - \vartheta_v)\cos(T + \Phi) + (1 \pm \delta)^2 S^{\pm}(T) \approx (1 - \vartheta_v)\cos T + \frac{\pi/4}{\delta}\sin T + \frac{1}{2}\left[T\sin T + \left(1 - \frac{\pi^2}{4}\right)\cos T\right] + \frac{\pi}{4}[\pm(T\cos T + \sin T)] \tag{C2}$$

Since the only odd function in T on $-\pi/2 < T < +\pi/2$ in (C2) is the term that varies inversely with δ, the only terms of order 1 in the Fourier series for the acceleration are odd harmonics of cosine functions. Writing

$$\frac{d}{dT}\left[\frac{(1 - \vartheta_v)v(T)}{V}\right] \approx \frac{\pi/4}{\delta}\sin T + \sum_{n=0}^{\infty}\alpha_{2n+1}\cos(2n + 1)T \tag{C3}$$

for T on $-\pi < T < +\pi$, one finds for $n > 0$

$$\alpha_{2n+1} = \frac{1}{4}\frac{(2n + 1)^2}{[n(n + 1)]^2} + n \qquad n \text{ even}$$
$$\alpha_{2n+1} = \frac{1}{4}\frac{(2n + 1)^2}{[n(n + 1)]^2} - (n + 1) \qquad n \text{ odd} \tag{C4}$$

Setting $n = 2k$ for $k = 1, 2, 3, \cdots$, one finds

$$\|\alpha_{2(2k+1)+1}| - |\alpha_{2(2k)+1}\| = \frac{1}{2}\frac{1}{(2k)(2k + 1)^2(2k + 2)} \approx \frac{1}{32}\frac{1}{k^4} \tag{C5}$$

where the asymptotic expression is intended for $k \gg 1$. Setting $n = 2k + 1$ for $k = 1, 2, 3, \cdots$, one finds that for large k

$$\|\alpha_{2(2k+1)+1}| - |\alpha_{2(2k+2)+1}\| \approx \frac{1}{32}\frac{1}{k^2} \tag{C6}$$

consequently, a "pairing" of amplitudes is obtained (see Figure 2). The pairing occurs fairly early in the series and becomes more pronounced. For example, for $n = 2, 3$ ($k = 1$ in (C4)) and $n = 4, 5$ ($k = 2$ in (C4))

$$|\alpha_7/\alpha_5| = 0.98, \qquad |\alpha_{11}/\alpha_9| \approx 0.996 \tag{C7}$$

while $|\alpha_7/\alpha_9| \approx 1.68$.

For $n = 0$, one obtains

$$\alpha_1 = (1 - \vartheta_v) + \left[1 - \left(\frac{\pi}{4}\right)^2\right] \tag{C8}$$

Acknowledgments. We thank Koen Van Den Abeele, Robert Guyer, Katherine McCall, Thomas Shankland, Patrick N. J. Rasolofosaon, and James Ten Cate for helpful discussions, and Michel Masson for experimental assistance. This work was performed under the auspices of the Offices of Basic Energy Research: Scientific Computing and Engineering and Geoscience, U.S. Department of Energy, with the University of California. Support was also provided by the Institut Français du Pétrole. We thank K. Van Den Abeele for critical review of the manuscript. We also are grateful to the two reviewers, who dramatically improved the manuscript.

References

Birch, F., Compressibility; Elastic constants, in *Handbook of Physical Constants*, edited by S. P. Clark, Jr., pp. 97–174, Geol. Soc. of Am., Boulder, Colo., 1966.

Boitnott, G. N., The role of rock joints in nonlinear attenuation, in *Proceedings of the Numerical Modeling for Underground Nuclear Test Monitoring Symposium*, edited by S. R. Taylor and J. R. Kamm, pp. 121–134, Los Alamos Natl. Lab., *Rep. LA-UR-93-3839*, 1993.

Gardner, G., M. R. Wyllie, and D. M. Droschak, Hysteresis in the velocity-pressure characteristics of rocks, *Geophysics*, *30*, 111–116, 1965.

Guyer, R. A., K. R. McCall, P. A. Johnson, P. N. J. Rasolofosaon, and B. Zinszner, Equation of state hysteresis and resonant bar measurements on rock, in *International Symposium on Rock Mechanics*, edited by J. J. K. Daemen and R. A. Schultz, pp. 177–181, A. A. Balkema, Rotterdam, Netherlands, 1995a.

Guyer, R. A., K. R. McCall, and G. N. Boitnott, Hysteresis, discrete memory and nonlinear wave propagation in rock, *Phys. Rev. Lett.*, *74*, 3491–3494, 1995b.

Holcomb, D. J., A quantitative model of dilitancy in dry rock, *J. Geophys. Res.*, *83*, 4941–4950, 1978.

Holcomb, D. J., Memory, relaxation, and microfracturing in dilatant rock, *J. Geophys. Res.*, *86*, 6235–6248, 1981.

Johnson, P. A., and P. N. J. Rasolofosaon, Manifestation of nonlinear elasticity in rock: Convincing evidence over large frequency and strain intervals from laboratory studies, *Nonlinear Processes Geophys.*, *3*, 77–88, 1996.

Johnson, P. A., B. Zinszner, and P. N. J. Rasolofosaon, Resonance and nonlinear elastic phenomena in rock, *J. Geophys. Res.*, *101*, 11,553–11,564, 1996.

Kadish, A., Information paths and the determination of state relations from displacement measurements of elastic rods, *J. Acoust. Soc. Am.*, *97*, 1489, 1995.

Kadish, A., J. Ten Cate, and P. A. Johnson, Frequency spectra of nonlinear pulse-mode waves, *J. Acoust. Soc. of Am.*, in press, 1996.

Lucet, N., and B. Zinszner, Effects of heterogeneities and anisotropy on sonic and ultrasonic attenuation in rocks, *Geophysics*, *57*, 1018–1026, 1992.

Meegan, G. D., P. A. Johnson, R. G. Guyer, and K. R. McCall, Observations of nonlinear elastic wave behavior in sandstone, *J. Acoust. Soc. Am.*, *94*, 3387–3391, 1993.

Ostrovsky, L. A., Wave processes in media with strong acoustic nonlinearity, *J. Acoust. Soc. Am.*, *90*, 3332–3337, 1991.

Stoker, J. J., *Nonlinear Vibrations in Mechanical and Electrical Systems*, vol. II, Interscience, New York, 1950.

Ten Cate, J., K. Van Den Abeele, T. J. Shankland, and P. A. Johnson, Laboratory study of linear and nonlinear elastic pulse propagation in sandstone, *J. Acoust. Soc. Am.*, in press, 1996.

Van Den Abeele, K. E.-A., and P. A. Johnson, Elastic pulsed wave propagation in media with second or higher order nonlinearity, II, Simulation of experimental measurements on Berea sandstone, *Jour. Acoust. Soc. Am.*, *99*, 3346–3352, 1996.

P. A. Johnson and A. Kadish, Earth and Environmental Sciences Division, Mail Stop D443, Los Alamos National Laboratory, Los Alamos, NM 87545. (e-mail: johnson@seismo5.lanl.gov; kadish@lanl.gov; URL: http://www.ees4.lanl.gov/nonlinear)

B. Zinszner, Institut Français du Pétrole, B.P. 311-92506, Rueil Malmaison Cedex, France. (e-mail: bernard.zinszner@ifp.fr)

(Received August 7, 1995; revised July 22, 1996;
accepted August 7, 1996.)